

Article

# SOC Estimation of E-Cell Combining BP Neural Network and EKF Algorithm

Yun Gao \*, Wujun Ji and Xin Zhao

College of Automotive Engineering, Henan Polytechnic, Zhengzhou 450046, China

\* Correspondence: gyauto@126.com

**Abstract:** Power lithium battery is an important core component of electric vehicles (EV), which provides the main power and energy for EV. In order to improve the estimation accuracy of the state of charge (SOC) of the electric vehicle battery (E-cell), the extended Kalman filter (EKF) algorithm, and backpropagation neural network (BPNN) are used to build the SOC estimation model of the E-cell, and the self-learning characteristic of BP neural network is used to correct the error and track the SOC of the E-cell. The results show that the average error of SOC estimation of BP-EKF model is 0.347%, 0.0231%, and 0.0749%, respectively, under the three working conditions of constant current discharge, pulse discharge, and urban dynamometer driving schedule (UDDS). Under the influence of different initial value errors, the average estimation errors of BP-EKF model are 0.2218%, 0.0976%, and 0.5226%. After the noise interference is introduced, the average estimation errors of BP-EKF model under the three working conditions are 1.2143%, 0.2259%, and 0.5104%, respectively, which proves that the model has strong robustness and stability. Using the BP-EKF model to estimate and track the SOC of E-cell can provide data reference for vehicle battery management and is of great significance to improve the battery performance and energy utilization of EV.

**Keywords:** back propagation neural network; extended Kalman filter; electric vehicle; state of charge



**Citation:** Gao, Y.; Ji, W.; Zhao, X. SOC Estimation of E-Cell Combining BP Neural Network and EKF Algorithm. *Processes* **2022**, *10*, 1721. <https://doi.org/10.3390/pr10091721>

Academic Editors: Jie Zhang and Meihong Wang

Received: 5 August 2022

Accepted: 25 August 2022

Published: 29 August 2022

**Publisher's Note:** MDPI stays neutral with regard to jurisdictional claims in published maps and institutional affiliations.



**Copyright:** © 2022 by the authors. Licensee MDPI, Basel, Switzerland. This article is an open access article distributed under the terms and conditions of the Creative Commons Attribution (CC BY) license (<https://creativecommons.org/licenses/by/4.0/>).

## 1. Introduction

Since the 21st century international energy consumption is increasing, the earth's oil resources are scarce, and there are serious environmental pollution problems, the global oil energy can not meet the needs of industry and automobiles and other aspects [1,2]. In recent years, due to the increasing sales of cars in China, the country's energy consumption has also shown a rapid growth trend. China is gradually becoming a net importer of non-renewable energy sources such as crude oil, coal, and natural gas in the world, and the external demand for energy is rising year by year, which has seriously affected China's energy security. In order to reduce environmental pollution and achieve the global goal of energy saving and emission reduction of greenhouse gases, the world and China's energy structure is also undergoing a series of changes, with the traditional fossil energy-based energy system gradually changing into a new supply system with renewable energy as the main source [3,4]. Traditional cars use petroleum as the main source of energy supply and emit a large amount of toxic exhaust gas during operation, further aggravating environmental pollution and degradation, so new energy vehicles powered by clean energy have become an important development direction for the automotive industry in recent years.

The remaining battery energy of an electric vehicle is an important parameter for battery management. The battery management system of an electric vehicle will use the remaining battery energy data as the basis to equalise the individual batteries, so as to improve the performance of battery use while ensuring stable battery operation. Accurate estimation of the remaining battery energy of EVs helps to reasonably allocate and plan the battery energy, develop scientific energy allocation strategies, ensure the driving range of EVs, and is of great value in extending the service life of EV batteries [5,6]. On the other

hand, the estimation of the remaining energy of EV can also play a protective role for the battery, avoiding the phenomenon of overcharging and over discharging, which accelerates the aging and elimination of the battery. Therefore, in order to further improve the service performance of electric vehicle batteries and strengthen the battery management, the extended Kalman filter algorithm and BP neural network are used to estimate the battery SOC and realize the accurate tracking of the battery SOC. It is expected to provide data support for the battery management system.

## 2. Related Works

The E-cell SOC of an electric vehicle directly affects the battery usage and daily driving of the vehicle, but the E-cell SOC is non-linear and cannot be measured directly, so many researchers have conducted research on the E-cell SOC estimation problem. A deep neural network with different number of hidden tiers was trained to predict the E-cell SOC under different driving cycles. It was found that the deep neural network with four hidden tiers could accurately predict the SOC under various operating conditions such as Dynamic Stress Test (DST) and Federal Urban Driving Schedule (FUDS) [7]. Xiong R and his team proposed a fractional-order discrimination model for E-cell based on least squares and nonlinear optimization by combining the Butler–Volmer equation and fractional-order calculus and used the model as the basis for estimating the E-cell SOC using the fractional-order traceless Kalman filter algorithm, which was further processed by singular value decomposition [8]. Sarrafan K et al. proposed a combined estimation model based on battery energy, adaptive forgetting factor recursive least squares for the non-linear E-cell SOC estimation problem, which solves the battery parameter rate variation problem while reducing the computational difficulty and fully considers the traffic environment and other conditions; after laboratory tests, the results showed that the combined SOC estimation model has high estimation accuracy [9]. He Z's group proposed to use the adaptive extended Kalman filter algorithm and adaptive recursive least squares for parameter identification and constructed a first-order RC equivalent circuit to identify the battery parameters using the estimation model with forgetting factors and dynamically adjust the system noise to improve the estimation accuracy of the model [10]. Wadi A et al. combined the extended Kalman filter algorithm and the smoothed variable structure filter algorithm to appraise the SOC state of lithium batteries, combining the robustness and noise sequence approximation advantages of the two algorithms to improve the accuracy of SOC estimation; experimental tests on different data sets showed that the model has high estimation accuracy and effectively reduces the computational complexity of the algorithm [11]. Many researchers use different methods to estimate the SOC state of electric vehicle batteries, but the estimation accuracy of the existing research needs to be improved. The research is expected to explore different estimation methods to further accurately track the battery SOC.

Kalman filter (KF) is a commonly used algorithm in the field of control, which has advantages in solving a variety of problems. Wul A et al. proposed a wind speed estimation model based on a Gaussian process regression model and an extended KF for the rotor effective wind speed estimation of wind turbines, taking into account the effects of other dynamics and atmospheric changes on the wind speed estimation; the results show that the model can effectively reduce the estimation errors arising from wind speed and other factors, and has high estimation accuracy [12]. Han F and his team proposed to use KF and random matrix theory for smart grid data-driven event detection in order to improve the power system's grid situational awareness and use dynamic KF to process the phasor measurement unit data; the research results show that the model has strong robustness [13]. Zhang Y et al. proposed a denoising algorithm based on composite Kalman and least squares curve fitting for the noise problem of marine sensors, using least squares to eliminate the nonlinear factors of the system and combining wavelet transform for real-time tracking of noise, using a combined model based on composite KF for sensor denoising to improve the temperature measurement accuracy of sensors [14]. Zhou T

et al. proposed a hybrid pairwise KF algorithm for predictive analysis of short-time traffic flow, modelled on the basis of the difference propagation between the traditional Kalman algorithm and the random wandering algorithm, and compensated for the prediction by means of error calibration, and the results of the study showed that the model has advantages on parametric and non-parametric models [15]. Li Y and his group members used magneto-optical imaging. The finite element model of the weld is combined with image characterisation of the weld to analyse the distribution of the leakage field under different conditions; in order to reduce the impact of weld coupling noise on the accuracy of laser weld analysis, the KF algorithm is used to identify the weld centre [16].

In summary, there are many studies on the SOC state estimation problem of E-cell, but the estimation accuracy needs to be further improved. Therefore, the study introduces BPNN and extended KF in the E-cell SOC estimation, expecting to further improve the SOC estimation accuracy of E-cell and provide help to improve the energy utilization efficiency of batteries.

### 3. Study on SOC Estimation of E-Cell Combining BP and EKF

#### 3.1. E-Cell Modelling

The battery system of the electric vehicle is the basis of the driving and operation of the electric vehicle. The battery management system of the vehicle can monitor and analyze the state of the vehicle battery, monitor and collect the voltage, temperature, and other parameters of the vehicle battery, and monitor the state of charge (SOC) of the battery, so as to facilitate the management of the battery energy and ensure the safe and stable operation of the power battery pack of the electric vehicle [17–19]. SOC is the remaining capacity data of the automobile battery. Accurate battery SOC data can provide a safe range for the charging and discharging of the automobile, promote the extension of the service life of the automobile battery, and directly affect the accuracy of the automobile mileage data [20,21]. The research studies the SOC estimation strategy of electric vehicles. Firstly, the lithium battery model of electric vehicles is established to provide a model basis for the subsequent SOC estimation of electric vehicles.

The research simulates the external dynamic response of the battery by establishing the equivalent circuit model of the automobile battery. In order to fully reflect the voltage current characteristics of the electric vehicle battery, the research uses the general nonlinear (GNL) equivalent circuit model to build the battery model of the electric vehicle. The study considers that although the high-order number model can improve the accuracy to a certain extent, it greatly increases the computational workload and complexity, so the study simplifies the high-order GNL model and uses the second-order RC ring model to simulate the battery circuit [22]. The second-order RC ring model of the battery is shown in Figure 1. Compared with the traditional GNL circuit, the second-order RC circuit has one less RC circuit, which can effectively maintain the non-linear characteristics of the battery and reduce the computational difficulty. The equivalent resistance of the battery is  $R_0$ , the open circuit voltage is  $E_0$ , the terminal voltage is  $v_0$ ,  $C_1$  and  $C_2$  represent the battery electrochemical polarisation capacitance and the concentration difference polarisation capacitance, respectively,  $R_1$  and  $R_2$  represent the battery electrochemical polarisation resistance and the concentration difference polarisation resistance, respectively, and  $V$  represents the battery open circuit voltage.

The terminal voltage and current functions for the second-order RC model of the battery are shown in Equation (1).

$$\begin{cases} v_0 = E_0 + v_1 + v_2 + iR_0 \\ i = \frac{v}{R} + C \frac{dv}{dt} \end{cases} \quad (1)$$

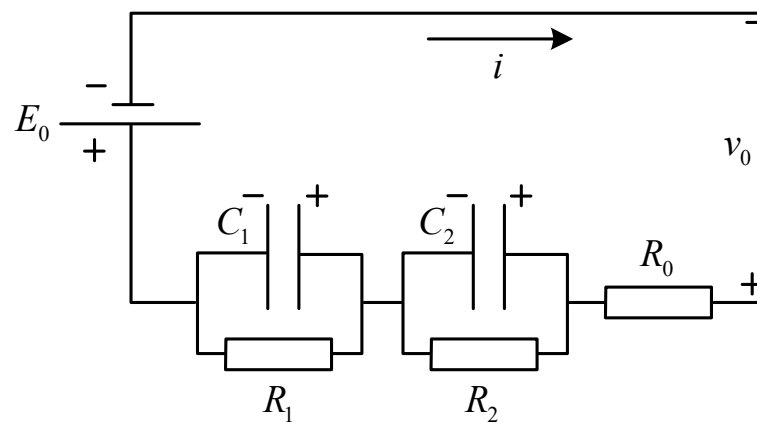


**Figure 1.** Second order RC ring model of battery.

In Equation (1),  $v_1$  and  $v_2$  represent the voltages at the ends of  $C_1$  and  $C_2$ , respectively. Using the E-cell SOC and capacitor terminal voltages as the state vectors of the system, the battery state space equations are shown in Equation (2).

$$\dot{x} = \begin{bmatrix} -\frac{1}{R_1 C_1} & 0 & 0 \\ 0 & -\frac{1}{R_2 C_2} & 0 \\ 0 & 0 & 0 \end{bmatrix} x + \begin{bmatrix} \frac{1}{C_1} \\ \frac{1}{C_2} \\ -\frac{1}{Q} \end{bmatrix} i \quad (2)$$

In Equation (2),  $x = [v_1 \ v_2 \ \text{SOC}]$ , and  $Q$  represents the battery capacity. The Eulerian method is used to discretize the continuous state equation, and the discretized state equation and system output equation are shown in Equation (3).

$$\begin{cases} x_k = \begin{bmatrix} -\frac{1}{R_1 C_1} \Delta t + 1 & 0 & 0 \\ 0 & -\frac{1}{R_2 C_2} \Delta t + 1 & 0 \\ 0 & 0 & 1 \end{bmatrix} x_{k-1} + \begin{bmatrix} \frac{\Delta t}{C_1} \\ \frac{\Delta t}{C_2} \\ -\frac{\Delta t}{Q} \end{bmatrix} i_{k-1} \\ v_{0,k} = E_{o,k} + v_{1,k} + v_{2,k} + i_k R_0 \end{cases} \quad (3)$$

### 3.2. EKF-Based E-Cell SOC Estimation

The Kalman filter (KF) algorithm is widely used in control applications and has a significant accuracy advantage in system estimation when the system noise satisfies the Gaussian distribution [23,24]. However, the classical Kalman filter is less suitable for non-linear systems and more suitable for linear systems, while EV have non-linear characteristics. The operation principle of the EKF model is shown in Figure 2. The EKF model is shown in Figure 2. The initialisation process is carried out first, then the battery state and error covariance are appraised, and the state appraises and error covariance values are updated by the extended Kalman filter gain calculation. Due to the strong robustness and adaptiveness of the EKF model, although the EKF model does not require a high degree of accuracy in terms of input battery parameters and initial SOC values, the EKF model can quickly achieve automatic convergence of the E-cell SOC during the computational update process, making it converge to the initial value, so the EKF model has a good and wide applicability for EV E-cell SOC estimation.

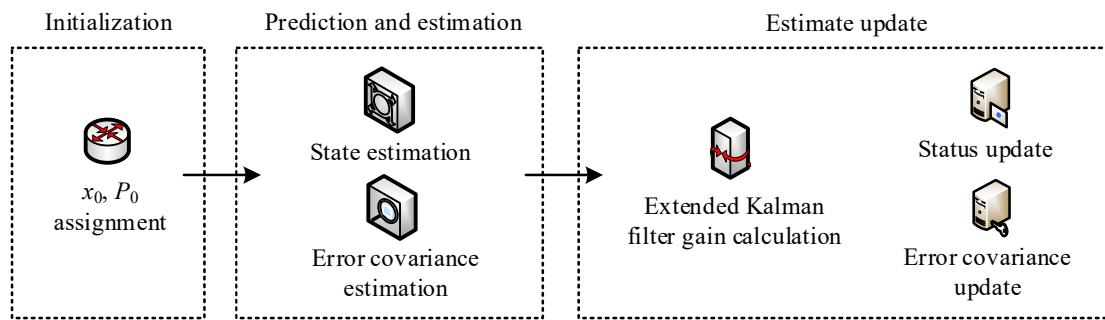


Figure 2. Operation principle of EKF model.

Let the inputs and outputs of the discrete system be  $u_k$  and  $y_k$ , respectively, and the system state quantities be  $x_k$ . The state transfer matrix of the system is  $A_k$ . The relationship between the inputs and states of the system is represented by  $B_k$ , and the observation and feedforward matrices of the system are  $C_k$  and  $D_k$ , respectively. Let the measurement noise and process noise of the system be  $v_k$  and  $w_k$ , respectively, and the noise is assumed to be Gaussian white noise with a mean value of 0. The discrete system function is shown in Equation (4).

$$\begin{cases} x_{k+1} = A_k x_k + B_k u_k + w_k \\ y_k = C_k x_k + D_k u_k + v_k \end{cases} \quad (4)$$

The EKF model is used for EV E-cell SOC estimation, where the state and observation equations of the system are Taylor expanded at the optimal estimation point, the higher order terms are discarded, the non-linear system is linearised, and the traditional KF algorithm is used for estimation. The state and observation equations of the system are shown in Equation (5).

$$\begin{cases} x_{k+1} = f(x_k, u_k) + w_k \\ y_k = h(x_k, u_k) + v_k \end{cases} \quad (5)$$

In Equation (5),  $f(x_k, u_k)$  and  $h(x_k, u_k)$  are the non-linear state transfer function and observation function, respectively. The state vector of the model is  $x = [v_1 \ v_2 \ SOC]^T$  and the input vector is  $u_k = i_k$ . The state transfer matrix and observation matrix of the system are shown in Equation (6).

$$\begin{cases} A_k = \frac{\partial f(x_k, u_k)}{\partial x_k} = \begin{bmatrix} -\frac{1}{R_1 C_1} \Delta t + 1 & 0 & 0 \\ 0 & -\frac{1}{R_2 C_2} \Delta t + 1 & 0 \\ 0 & 0 & 1 \end{bmatrix} \\ C_k = \frac{\partial h(x_k, u_k)}{\partial x_k} = \begin{bmatrix} 1 & 1 & \frac{\partial E_0}{\partial SOC} \end{bmatrix} \end{cases} \quad (6)$$

Further estimation is performed using the KF algorithm by first initialising, at this point  $k = 0$ , assigning values to the system state initial value  $x_0$  and the error writing covariance  $P_0$ . The a priori values of the system state quantities are then appraised using the model inputs and the best appraise of the system state at the previous moment, and the estimation function for the system state quantities at the current moment is shown in Equation (7).

$$x_k^- = A_{k-1} x_{k-1} + B_{k-1} u_{k-1} \quad (7)$$

The initial value error will have an impact on the accuracy of the a priori appraise of the system state. To ensure that the a priori appraise accurately tracks the true value, the degree of dispersion between the appraise and the true value is analysed through the calculation of the error covariance. The current moment value is appraised using the error covariance of the previous moment, and the error covariance calculation function is shown in Equation (8).

$$P_k^- = A_{k-1} P_{k-1} A_{k-1}^T + Q_{k-1} \quad (8)$$

In Equation (8), the covariance matrix of the process noise is represented. The correction factor for the appraised value is obtained from the error covariance, i.e., the Kalman gain matrix. The extended Kalman gain calculation function is shown in Equation (9).

$$L_k = P_k^- C_k^T [P_k^- C_k^T + R_w]^{-1} \tag{9}$$

In Equation (9),  $Q_k$  is the covariance matrix of the measurement noise. The a priori appraisals are updated in combination with the gain to obtain the best a priori appraisal, and the system state appraisal update function is shown in Equation (10).

$$x_k = x_k^- + L_k (y_k - C_k x_k^- - D_k u_k) \tag{10}$$

In Equation (10),  $y_k$  is the measured value of the system state quantity at the current moment. The error covariance of the system is updated, and the update function is shown in Equation (11).

$$P_k = (I - L_k C_k) P_k^- \tag{11}$$

In Equation (11),  $I$  is the unit matrix.

### 3.3. Optimization of Estimation Models Based on BP Neural Networks

In order to improve the estimation accuracy of the EKF model, the BPNN was used to compensate for the error, and the self-learning characteristics of the BPNN and its ability to approximate nonlinear functions were used to further optimize the EKF model. The EKF model is shown in Figure 3. The SOC state quantities at  $k$ ,  $v_1$ , and  $v_2$  and the gain values calculated by the EKF model are used as the input values of the BPNN, and the BPNN is used to output the error compensation values to correct the appraised values.

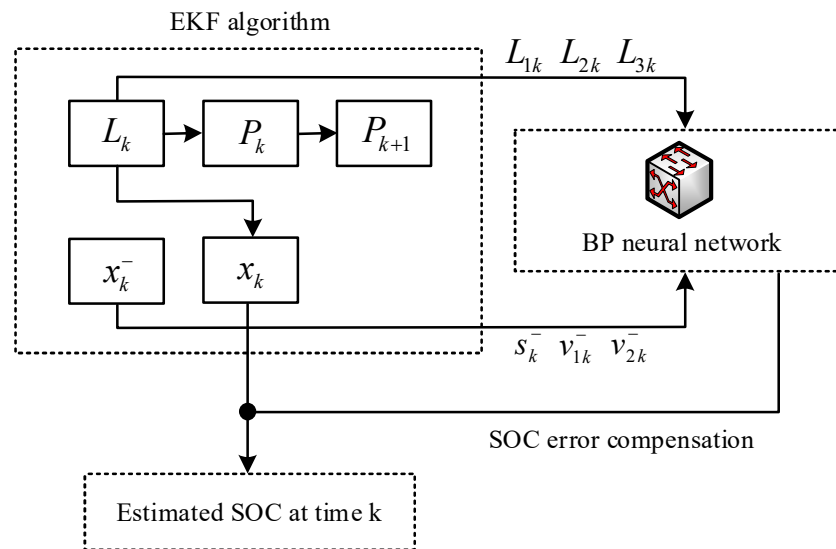


Figure 3. Structure of BP-EKF model.

Due to the variation in the range of E-cell SOC, voltage and gain values, and the different magnitudes and orders of magnitude of the individual input and output data, the input and output data are first normalised so that the data are between [1] to ensure that the sample data are weighted differently by the influence in training and to avoid the problem of neuron saturation, which affects the training effect of the network model. The normalisation function for the input and output data is shown in Equation (12).

$$\begin{cases} \bar{x}_i = \frac{x_i - x_{\min}}{x_{\max} - x_{\min}} \\ \bar{x}_{ii} = 2 \times \frac{x_{ii} - x_{\min}}{x_{\max} - x_{ii}} - 1 \end{cases} \tag{12}$$

Using the battery state quantity and Kalman filter coefficients as the input values of the BPNN, the input quantity of the BPNN is  $x_i = [v_1 \ v_2 \ SOC \ k_1 \ k_2 \ k_3]$ . The input quantity of the output tier of the BPNN  $x_l$  is the weighted sum of the output of the hide tier, while the excitation function of the output quantity  $x'_l$  is the tansig function with the function value range of  $(-1, 1)$ . The input quantity and output quantity of the output tier are shown in Equation (13).

$$\begin{cases} x_l = \sum w_{jl} x'_j \\ x'_l = \frac{2}{1+e^{-2x_l}} - 1 \end{cases} \quad (13)$$

The algorithm for learning the connection weights between the implicit and import tiers of the BPNN, and the connection weights to the output tier, is shown in Equation (14).

$$\begin{cases} \Delta w_{ij} = \eta \cdot e \cdot w_{jl} \cdot f'(x'_j) \cdot x_i \\ \Delta w_{jl} = \eta \cdot e \cdot x'_j \end{cases} \quad (14)$$

In Equation (14),  $\eta$  denotes the learning rate,  $\eta \in [0, 1]$ , and  $e$  denotes the error of the output value from the ideal value. In order to solve the problem of model oscillation or slow convergence of BPNN in weight learning, the momentum factor  $\alpha$  is introduced for adjustment,  $\alpha \in [0, 1]$ , fully considering the influence of the previous moment weights on the present weights, then the weights  $w_{ij}$  and  $w_{jl}$  are shown in Equation (15).

$$\begin{cases} w_{ij}(k+1) = w_{ij}(k) + \Delta w_{ij} + \alpha(w_{ij}(k) - w_{ij}(k-1)) \\ w_{jl}(k+1) = w_{jl}(k) + \Delta w_{jl} + \alpha(w_{jl}(k) - w_{jl}(k-1)) \end{cases} \quad (15)$$

The role of the implicit layer of the BPNN is to extract and store the laws in the sample data. The implicit layer directly affects the mapping ability of the network; too many nodes in the implicit layer may lead to overfitting problems and affect the network generalization ability, while too few nodes will affect the extraction of the sample laws. The estimation function of the number of nodes in the hide tier is shown in Equation (16).

$$\begin{cases} m = \sqrt{n+1} + \alpha \\ m = \log_2 n \\ m = \sqrt{nl} \end{cases} \quad (16)$$

In Equation (16),  $n$  and  $l$  denote the number of nodes in the input and output tiers, respectively,  $\alpha$  is a constant, and  $\alpha \in [1, 10]$ .

#### 4. Analysis of the Application Effect of the BP-EKF Based E-Cell SOC Estimation Model

##### 4.1. Validation of Battery Modelling Effects

In order to verify the response effect of the electric vehicle battery model constructed in the research on the dynamic characteristics of the battery, the equivalent circuit model of the battery was built in the Simulink environment. The input and output of the battery model were circuit current and terminal voltage, respectively. The rated capacity of the battery was 20 Ah, the maximum discharge current was 100 A, the maximum charging voltage was 4.15 V, and the cut-off voltage was 3 V. The electrochemical polarization resistance and concentration difference polarization resistance of the battery are 0.0042  $\Omega$  and 0.0020  $\Omega$ , respectively, the equivalent resistance of the battery is 0.0013  $\Omega$ , and the electrochemical polarization capacitance and concentration difference polarization capacitance of the battery are 17,111 F and 440.56 F, respectively. The output data of the battery model under DST working condition is compared with the actual data of the battery, and the reflecting ability of the dynamic characteristics of the battery model is analyzed. The comparison between the output data of the battery model and the actual data is shown in Figure 4.

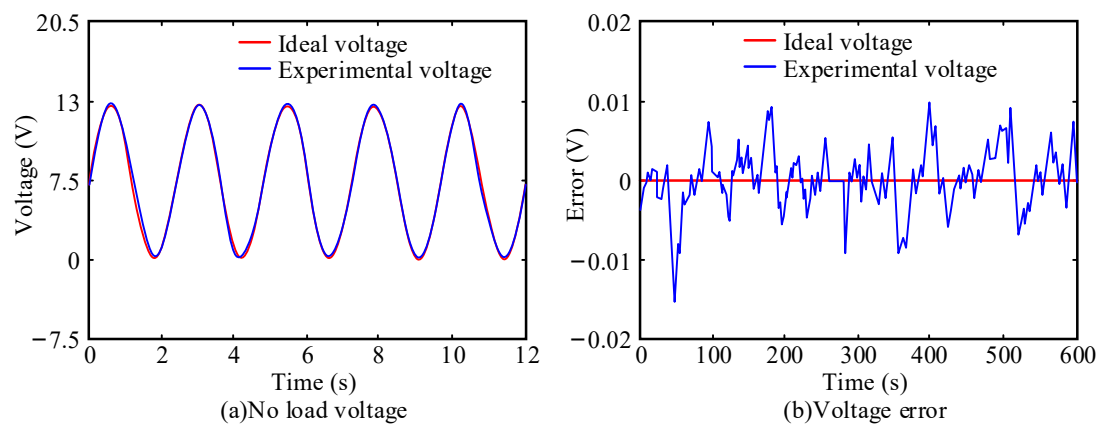


**Figure 4.** No load discharge test of battery.

Figure 4a shows the results of the battery no-load voltage test, and it can be seen that the ideal no-load voltage required for the study is 13 V, and the voltage value exhibited by the battery during the experiment is also 13 V, i.e., the state of the experimental voltage under no-load is consistent with the ideal value. Figure 4b shows the error variation between the experimental voltage and the ideal voltage in the battery discharge test. It can be seen that there is significant error variation between the experimental voltage and the ideal voltage during the 600 s test time, but it is known from the error magnitude of the experimental voltage that the maximum error voltage is only 0.015 V, and the error stays within 0.005 V for most of the time. The above results show that the proposed BP-EKF battery has a high agreement with the ideal voltage under no-load condition and during the discharge process, indicating that the BP-EKF-based battery design is reasonable.

#### 4.2. Analysis of the Estimation Accuracy of the BP-EKF Model

In order to verify the accuracy of the BP-EKF model constructed in the study for E-cell SOC estimation and to investigate the validity and feasibility of the model, the study was carried out in the MATLAB/SIMULINK working environment to simulate the battery operating mode for experiments. The battery is assumed to be fully charged at the initial moment, the initial value of SOC is set to 1, the battery current is 0, and the terminal voltage at both ends of the RC circuit is 0. Therefore, the initial values of the states are  $[0 \ 0 \ 1]$  and  $R = 1000$ . The operating effects of the model under constant current discharge, pulse discharge, and UDDS conditions are analysed, respectively. The SOC estimation and error of the model under constant current discharge conditions are shown in Figure 5.

As can be seen from Figure 5, the model's SOC appraisals are very close to the true values under constant current discharge conditions, and the model is able to converge accurately and quickly to approximate the true values, with a maximum error of 0.22% and an average error of 0.347% between the model's SOC appraisals and the true values' accuracy. The SOC estimation results and errors of the model under pulse discharge conditions are shown in Figure 6.

As can be seen in Figure 6, the difference between the appraised and true values of the EV E-cell SOC using the model under pulse discharge conditions is small, and the model is able to converge to the true value quickly, with a maximum error of 1.0367% and an average error of 0.0231% in the model SOC estimation. The results and errors of the model E-cell SOC estimation under UDDS conditions are shown in Figure 7.

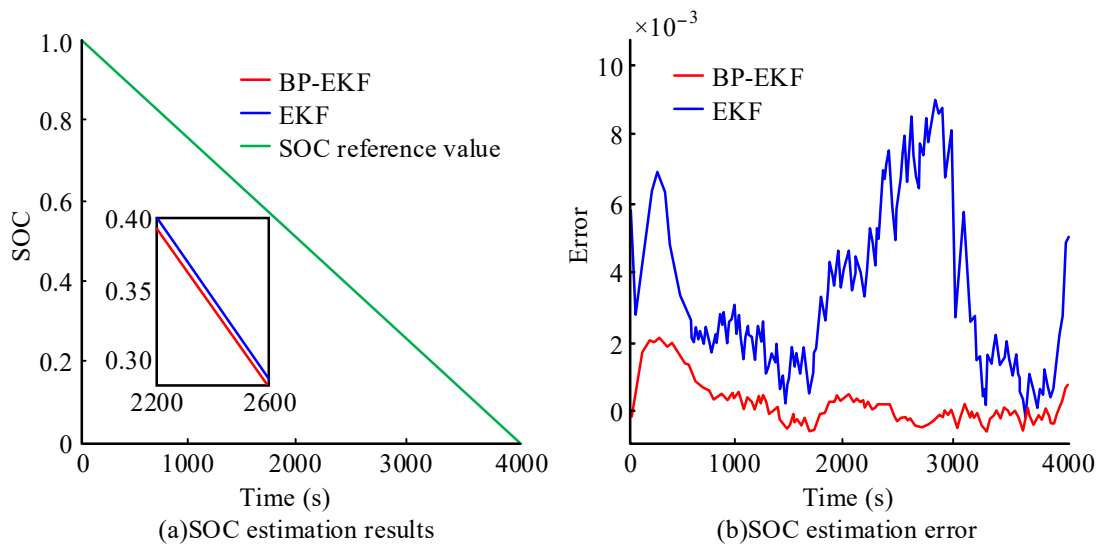


Figure 5. SOC estimation and error of the model under constant current discharge condition.

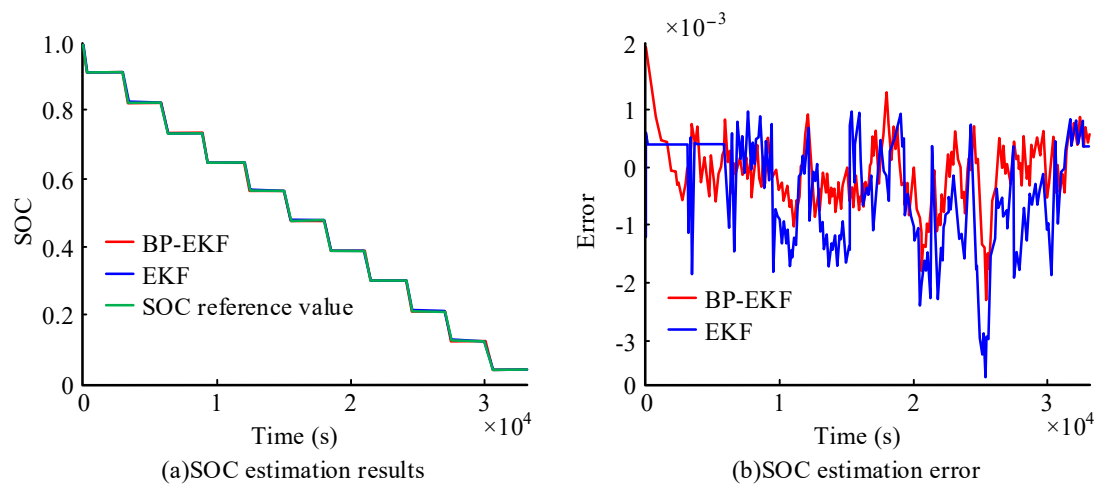


Figure 6. SOC estimation results and errors of the model under pulse discharge conditions.

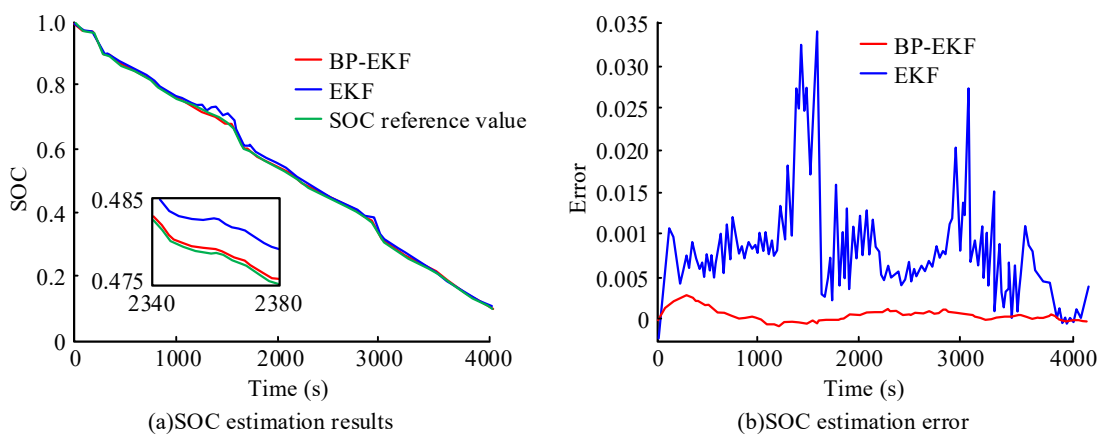
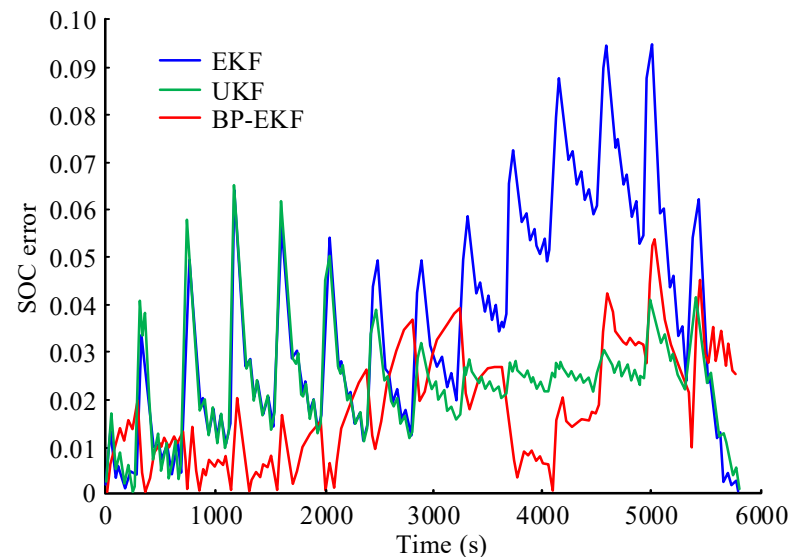


Figure 7. SOC estimation results and errors of model battery under UDDS conditions.

As can be seen from Figure 7, the model converges quickly to the true value in the UDDS condition, and the difference between the appraised SOC and the true value is small. Compared with the constant current discharge condition and the pulse discharge

condition, the estimation error of the model under UDDS condition increases slightly, but still maintains a good estimation accuracy. The BP-EKF model was compared with the unscented Kalman filter (UKF) model and the EKF model, and the absolute value of the estimation error of the E-cell SOC for the DST condition is shown in Figure 8.



**Figure 8.** Absolute value curve of E-cell SOC estimation error of three models under DST operating mode.

As can be seen in Figure 8, during the time period 0–3000 s, when the battery is in a stable state of low current charging and discharging, all three models have a small error in estimating the E-cell SOC and can better appraise the E-cell SOC situation accurately. At 3000 s, when the battery has a sudden change in current, the EKF and UKF models are unable to track the state quantity quickly and accurately, resulting in a sudden increase in the SOC estimation error, and the SOC estimation error curves of the EKF and UKF models show large fluctuations and rising trends. The estimation error of the EKF model gradually becomes larger and the estimation performance is less stable. In contrast, the BP-EKF model, with the effect of BPNN and extended Kalman filter gain, always maintains a low level of E-cell SOC estimation error, and after a sudden current change at 3000 s, the estimation error of the model falls back quickly, and the error curve fluctuates less.

#### 4.3. Robustness Analysis of the BP-EKF Model

During the initial start-up of an electric vehicle, it is difficult for the battery management system to obtain the initial value of the E-cell SOC. The E-cell SOC estimation model is required to provide fast and accurate tracking of the true value of the SOC when the initial value of the SOC is clear, and also needs to converge quickly to the true value when the initial value is unknown to ensure the accuracy and efficiency of the SOC value estimation. In order to investigate the adaptability of the BP-EKF model proposed in the study to the case of unknown initial SOC values and to analyse the convergence capability of the model, the study analyses the estimation performance of the model under different initial SOC values. Ensuring that other parameters are the same, the range of SOC initial values is set to [0.5, 1], the division interval is 0.1, and the model estimation results for six SOC initial value cases are shown in Figure 9.

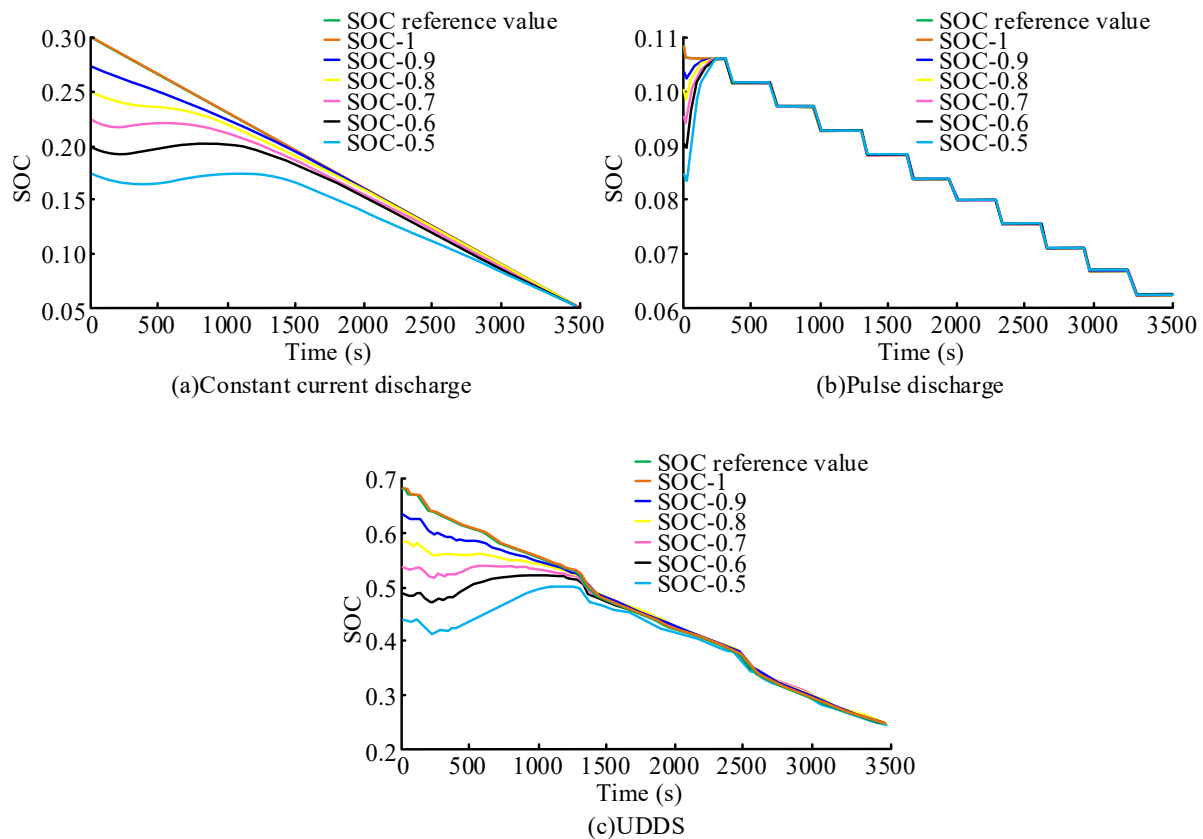


**Figure 9.** Model estimation effect under six initial SOC values.

It can be seen from Figure 9 that under the constant current discharge condition, the model proposed by the research is used to estimate the SOC of the battery. When the initial value of SOC is different from the actual value to different degrees, the average SOC estimation error of the model is 0.2218% under the six initial values of SOC, while the average SOC estimation error under the pulse discharge condition is 0.0976%. Under UDDS working condition, the average error of SOC estimation of the model battery is 0.5226%, which can meet the actual application requirements of battery management of electric vehicles. It proves that the BP-EKF model can effectively track the SOC of the battery quickly and accurately.

In order to verify the adaptability of the proposed model to current noise, the SOC estimation results of the BP-EKF model and the EKF model under three operating conditions were compared and analysed in a simulation environment with a white noise with a mean square deviation of  $10A^2$  to investigate the robustness and optimisation of the model.

From Figure 10, it can be seen that after adding noise to the current signal, the average estimation error values of the BP-EKF model are 1.2143%, 0.2259%, and 0.5104%, respectively, for the three operating conditions, while the average error values of the EKF model are 2.2416%, 0.9968%, and 2.1864%, respectively, which proves that the BP-EKF model can effectively cope with the noise interference, and the SOC estimation error of the BP-EKF model is smaller with the error compensation of the BPNN.

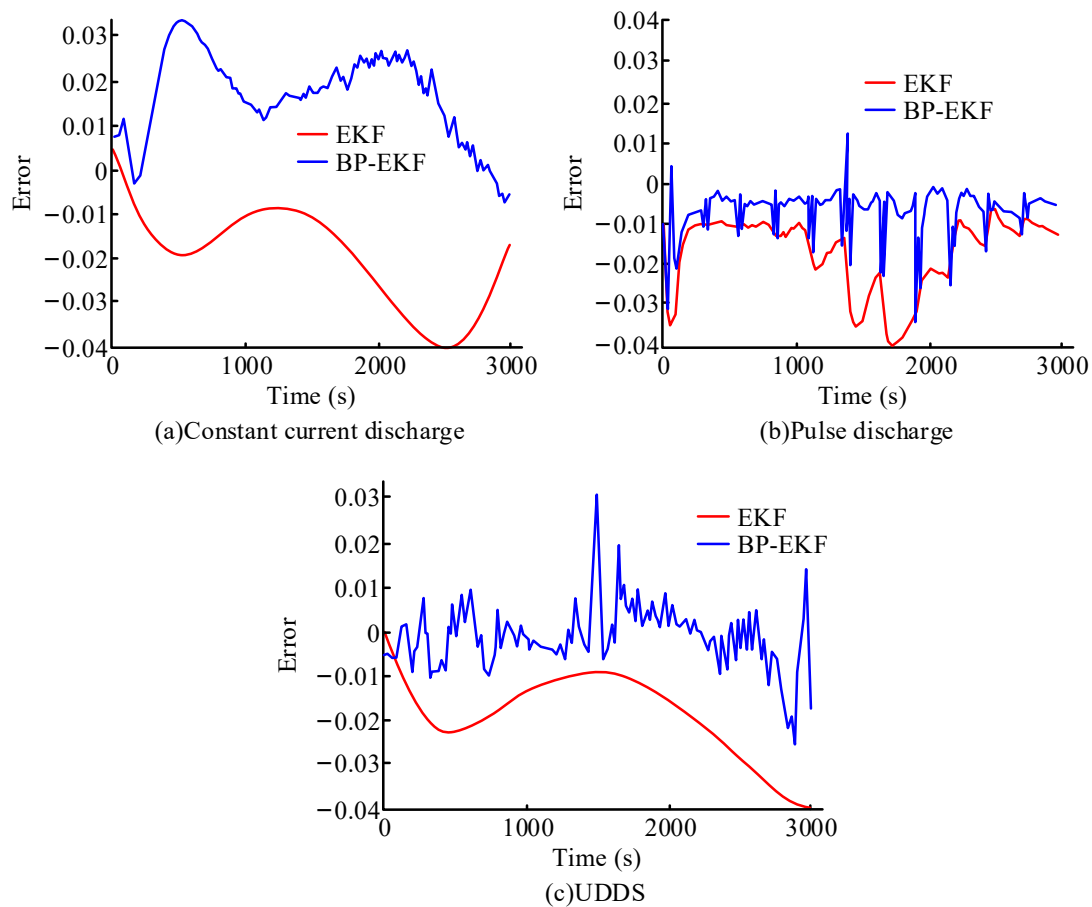


**Figure 10.** Model estimation effect under six initial SOC values (EKF and BP-EKF model).

## 5. Conclusions

In order to make accurate estimation of E-cell SOC, the study uses the extended Kalman filter algorithm to construct an E-cell SOC estimation model and introduces BPNN to compensate the error of the SOC estimation model to achieve accurate and fast tracking of E-cell SOC. The study conducts simulation experiments in the MATLAB/SIMULINK working environment. The experimental results show that the average errors between the BP-EKF model SOC estimation and the real value are 0.347%, 0.0231%, and 0.0749% under the three operating conditions of constant current discharge, pulse discharge, and UDDS. The average SOC estimation errors of the BP-EKF model for different initial values were 0.2218%, 0.0976%, and 0.5226%, proving that the model is more applicable to different initial value errors. The average estimation errors of the BP-EKF model under noise disturbance were 1.2143%, 0.2259%, and 0.5104%, proving that the model has strong robustness. The study analyses the model performance under three operating conditions, and in the future, the influence of temperature and other factors can be further considered to optimise the E-cell SOC estimation under a variety of operating conditions.

**Author Contributions:** Conceptualization, Y.G.; data curation, X.Z.; formal analysis, W.J.; investigation, W.J.; methodology, Y.G.; project administration, Y.G.; software, W.J.; validation, X.Z.; writing—original draft, Y.G.; writing—review & editing, Y.G. All authors have read and agreed to the published version of the manuscript.

**Funding:** This research received no external funding.

**Institutional Review Board Statement:** Not applicable.

**Informed Consent Statement:** Not applicable.

**Data Availability Statement:** The data used to support the findings of this study are available from the corresponding author upon request.

**Conflicts of Interest:** The authors declare no conflict of interest.

## References

1. Bi, J.; Wang, Y.; Sai, Q.; Ding, C. Estimating remaining driving range of battery EV based on real-world data: A case study of Beijing, China. *Energy* **2019**, *169*, 833–843. [[CrossRef](#)]
2. Chen, X.; Lei, H.; Xiong, R.; Shen, W.; Yang, R. A novel approach to reconstruct open circuit voltage for state of charge estimation of lithium ion batteries in EV. *Appl. Energy* **2019**, *255*, 113758. [[CrossRef](#)]
3. How, D.N.; Hannan, M.A.; Lipu, M.H.; Ker, P.J. State of charge estimation for lithium-ion batteries using model-based and data-driven methods: A review. *IEEE Access* **2019**, *7*, 136116–136136. [[CrossRef](#)]
4. Kim, W.; Lee, P.Y.; Kim, J.; Kim, K.S. A robust state of charge estimation approach based on nonlinear battery cell model for lithium-ion batteries in EV. *IEEE Trans. Veh. Technol.* **2021**, *70*, 5638–5647. [[CrossRef](#)]
5. Zhang, Y.; Chu, L.; Ding, Y.A.N.; Xu, N.A.N.; Guo, C.; Fu, Z.; Xu, L.; Tang, X.; Liu, Y. A hierarchical energy management strategy based on model predictive control for plug-in hybrid EV. *IEEE Access* **2019**, *16*, 2303–2308.
6. Wang, C.; Yang, R.; Yu, Q. Wavelet transform based energy management strategies for plug-in hybrid EV considering temperature uncertainty. *Appl. Energy* **2019**, *256*, 113928. [[CrossRef](#)]
7. How, D.N.; Hannan, M.A.; Lipu, M.S.H.; Sahari, K.S.; Ker, P.J.; Muttaqi, K.M. State-of-charge estimation of li-ion battery in EV: A deep neural network approach. *IEEE Trans. Ind. Appl.* **2020**, *56*, 5565–5574. [[CrossRef](#)]
8. Xiong, R.; Tian, J.; Shen, W.; Sun, F. A novel fractional order model for state of charge estimation in lithium ion batteries. *IEEE Trans. Veh. Technol.* **2019**, *68*, 4130–4139. [[CrossRef](#)]
9. Sarrafan, K.; Muttaqi, K.M.; Sutanto, D. Real-time estimation of model parameters and state-of-charge of li-ion batteries in EV using a new mixed estimation model. *IEEE Trans. Ind. Appl.* **2020**, *56*, 5417–5428. [[CrossRef](#)]
10. He, Z.; Yang, Z.; Cui, X.; Li, E. A method of state-of-charge estimation for EV power lithium-ion battery using a novel adaptive extended Kalman filter. *IEEE Trans. Veh. Technol.* **2020**, *69*, 14618–14630. [[CrossRef](#)]
11. Wadi, A.; Abdel-Hafez, M.F.; Hussein, A.A.; Alkhwaja, F. Alleviating dynamic model uncertainty effects for improved e-cell soc estimation of EVs in highly dynamic environments. *IEEE Trans. Veh. Technol.* **2021**, *70*, 6554–6566. [[CrossRef](#)]
12. Whl, A.; Al, A.; Fm, A. Real-time rotor effective wind speed estimation using Gaussian process regression and Kalman filtering. *Renew. Energy* **2021**, *169*, 670–686.
13. Han, F.; Ashton, P.M.; Li, M.; Pisica, I.; Taylor, G.; Rawn, B.; Ding, Y. A data driven approach to robust event detection in smart grids based on random matrix theory and kalman filtering. *Energies* **2021**, *14*, 2166. [[CrossRef](#)]
14. Zhang, Y.; Wang, R.; Li, S.; Qi, S. Temperature sensor denoising algorithm based on curve fitting and compound kalman filtering. *Sensors* **2020**, *20*, 1959. [[CrossRef](#)]
15. Zhou, T.; Jiang, D.; Lin, Z.; Han, G.; Xu, X.; Qin, J. Hybrid dual Kalman filtering model for short-term traffic flow forecasting. *IET Intell. Transp. Syst.* **2019**, *13*, 1023–1032. [[CrossRef](#)]
16. Mo, Y.; Song, Z.; Li, H.; Jiang, Z. A hierarchical safety control strategy for exoskeleton robot based on maximum correntropy kalman filter and bounding box. *Robotica* **2019**, *37*, 2165–2175. [[CrossRef](#)]
17. Li, Y.; Gao, X.; Chen, Y.; Zhou, X.; Zhang, Y.; You, D. Modeling for tracking micro gap weld based on magneto-optical sensing and kalman filtering. *IEEE Sens. J.* **2020**, *21*, 11598–11614. [[CrossRef](#)]
18. Esfandyari, M.J.; Esfahanian, V.; Yazdi, M.H.; Nehzati, H.; Shekoofa, O. A new approach to consider the influence of aging state on Lithium-ion battery state of power estimation for hybrid EV. *Energy* **2019**, *176*, 505–520. [[CrossRef](#)]
19. Yu, D.; Ma, Z.; Wang, R. Efficient smart grid load balancing via fog and cloud computing. *Math. Probl. Eng.* **2022**, *2022*, 3151249. [[CrossRef](#)]
20. Wang, S.; Lu, L.; Han, X.; Ouyang, M.; Feng, X. Virtual-battery based droop control and energy storage system size optimization of a DC microgrid for electric vehicle fast charging station. *Appl. Energy* **2020**, *259*, 114146. [[CrossRef](#)]
21. Singh, B.; Kushwaha, R. Power factor pre-regulation in interleaved Luo converter fed e-cell charger. *IEEE Trans. Ind. Appl.* **2021**, *57*, 2870–2882. [[CrossRef](#)]
22. Yu, D.; Wu, J.; Wang, W.; Gu, B. Optimal performance of hybrid energy system in the presence of electrical and heat storage systems under uncertainties using stochastic p-robust optimization technique. *Sustain. Cities Soc.* **2022**, *83*, 103935. [[CrossRef](#)]
23. Li, X.; Wang, Z.; Zhang, L. Co-estimation of capacity and state-of-charge for lithium-ion batteries in EV. *Energy* **2019**, *174*, 33–44. [[CrossRef](#)]
24. Hannan, M.A.; How, D.N.; Lipu, M.H.; Ker, P.J.; Dong, Z.Y.; Mansur, M.; Blaabjerg, F. SOC estimation of li-ion batteries with learning rate-optimized deep fully convolutional network. *IEEE Trans. Power Electron.* **2020**, *36*, 7349–7353. [[CrossRef](#)]